ACS APPLIED MATERIALS & INTERFACES

Letter

www.acsami.org

Stabilized CdSe-CoPi Composite Photoanode for Light-Assisted Water Oxidation by Transformation of a CdSe/Cobalt Metal Thin Film

Ronny Costi,*[,†,‡] Elizabeth R. Young,[‡,§] Vladimir Bulović,[‡] and Daniel G. Nocera*[,†,⊥]

[†]Department of Chemistry and [‡]Organic and Nanostructured Electronics Laboratory, Department of Electrical Engineering and Computer Science, Massachusetts Institute of Technology, 77 Massachusetts Avenue, Cambridge, Massachusetts 02139, United States

Supporting Information

ABSTRACT: Integration of water splitting catalysts with visible-light-absorbing semiconductors would enable direct solar-energy-to-fuel conversion schemes such as those based on water splitting. A disadvantage of some common semiconductors that possess desirable optical bandgaps is their chemical instability under the conditions needed for oxygen evolution reaction (OER). In this study, we demonstrate the dual benefits gained from using a cobalt metal thin-film as the precursor for the preparation of cobalt-phosphate (CoPi) OER catalyst on cadmium chalcogenide photoanodes. The cobalt layer protects the underlying semiconductor from oxidation and degradation while forming the catalyst and simultaneously facilitates the advantageous incorporation of the cadmium chalcogenide layer into the CoPi layer during continued processing of the electrode. The resulting hybrid material forms a stable photoactive anode for light-assisted water splitting.

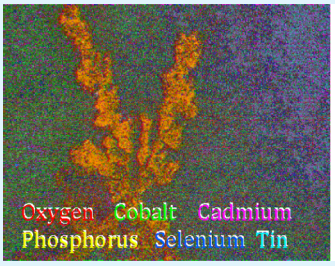

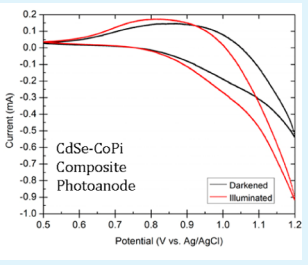

KEYWORDS: *catalysis, water oxidation, water splitting, solar fuels, electrochemistry, composite electrodes*

Efficient sunlight-driven splitting of water into molecular oxygen and hydrogen is a challenging target for direct solar-energy-to-fuels production.[1−4] For this objective to be achieved, two conditions are necessary: (1) efficient utilization of the solar spectrum for photon to charge conversion, and (2) execution of the four proton, four electron proton-coupled electron transfer reaction of water splitting at low overpotential. The first requirement can be addressed by using semiconducting materials that suitably absorb in the visible range, such as cadmium chalcogenides. However, many of these materials, including CdSe, are oxidatively unstable to the conditions needed for the oxygen evolution reaction (OER), rendering them unusable for water splitting purposes.[5] The second requirement demands the development of catalysts that promote the two half-reactions of the OER and hydrogen evolution reaction (HER). Of the two, the OER is particularly demanding because it requires the coupling of multiple proton and electron transfers, the distribution of four redox processes over a narrow potential range, and the formation of two oxygen−oxygen bonds.[6−9]

A cobalt−-phosphate-based OER catalyst (CoPi) has been found to be particularly effective for water-splitting under simple and chemically benign conditions.[10] The CoPi catalyst facilitates water oxidation by lowering the overpotential needed (<400 mV) at appreciable current densities (up to 100 mA/cm^2).[11] The CoPi catalyst can be prepared by various methods, including electrochemical (or photoelectrochemical) deposition from a solution of ionic precursors[10,12] or by electrochemical transformation of solid-state sputtered cobalt metal thin-films.[13] Both methods result in similar materials but the second method has the advantage of directly furnishing a protective layer of the underlying electrode, thus preventing its exposure to the aqueous solution and OER chemistry.[14]

The CoPi catalyst has been integrated to semiconductor light harvester materials comprising metal oxides, including ZnO,[15] WO_3[16] and Fe_2O_3,[17−21] which are stable under oxidizing conditions. But most of these materials are wide band gap semiconductors and their spectral coverage of the solar spectrum occurs primarily in the UV range. Silicon has also been used, in combination with CoPi, for a water oxidation scheme.[14,22,23] In these cases, to prevent oxidation of the silicon into insulating SiO_2, a thin protecting film of a conducting metal oxide (ITO) or cobalt metal were placed atop the silicon surface. For the latter, the cobalt layer was sputtered onto the silicon and converted directly to the CoPi catalyst while minimizing the oxidation of the silicon.[14]

Forming CoPi on top of CdSe electrodes, through transformation of a top cobalt metal thin film, can both protect the CdSe during electrode processing and allow a visible-light absorbing semiconductor to be coupled to the CoPi catalyst for more efficient photoassisted water oxidation. CdSe films were prepared on 1 × 2 cm^2 fluorine-doped tin

Received: January 27, 2013
Accepted: March 22, 2013
Published: March 22, 2013

oxide (FTO) covered glass substrates (TEC7, Hartford Glass) before an overlaying layer of cobalt was added to the complete unprocessed electrode structure. The FTO substrates were cleaned by sonication in acetone, immersed in boiling isopropanol and dried under dry N_2 flow. The CdSe layer was prepared as described elsewhere.[24] In short, a precursor solution was prepared by dissolving 0.2 mmol of cadmium chloride (99.998%, Alpha Aesar) and 0.2 mmol of selenourea (99.5+%, Alpha Aesar) in 8 mL of butylamine (99.5%, Sigma-Aldrich). The solution was placed in an ultrasonic bath for 1 min after which it turned light yellow. The solution was spin-coated at 1500 rpm on the cleaned FTO substrate and annealed at 100 °C under vacuum (~1×10^{-3} Torr) for between 1 and 3 h. The resulting CdSe sample was a rough, multicrystalline brown-red film. Cobalt metal was sputtered onto the CdSe film using an AJA sputter chamber to complete the sample structure (see figure S1 in the Supporting Information for an Auger cross-section of the unprocessed electrode). Cobalt film thicknesses ranged from 150 to 800 nm. The sample was then masked using an insulating lacquer, exposing a 1 cm^2 area. Processing of the cobalt metal was performed using a 3-electrode setup and by applying 1.3 V vs Ag/AgCl to the working electrode (the unprocessed FTO/CdSe/Co sample) in electrolyte solution for various amounts of time, typically 8−12 h. The electrolyte solution consisted of a phosphate buffer at pH 7, with concentrations ranging from 0.1 M for electrodes with an 800 nm thick cobalt layer to 0.025 M for electrodes with 150−300 nm thick cobalt layer.

Figure 1 shows the results of the different and complementary characterizations of the processed electrodes. In order to ascertain a depth profile of the composition of the electrode, a crater was formed in the processed electrode by sputter-ablation with an Ar^+ ion beam. The FTO substrate is exposed in the center of the crater, and the sides of the crater slope from top to bottom to reveal the intermediate layers. This preparation allows for the characterization of the chemical content throughout the sample. SEM was used to visually determine the existence of the CoPi catalyst layer on the surface of the sample. Figure 1a is a SEM image of the crater formed on a sample using the Ar^+ ion beam. This sample was transformed through a 12 h electroprocessing of the cobalt metal film. The top layer of the sample (as shown on the left of the image) exhibits the distinguishing nodules and cracks that are familiar to previous studies of CoPi (see Figures S2 and S3 in the Supporting Inforamtion for SEM images of the processed top layer surface).

The elemental content of the samples was characterized by several complementary methods. Auger Electron Spectroscopy (AES) measurements were taken to analyze the elemental content during formation of the crater. The calibrated AES profile provides an atomic concentration profile of the different elements in the sample. Also, the AES data may be used to differentiate between the chemical states and environments of the detected elements by observing shifts in the energy of the Auger peaks. This technique discriminates between the compounds formed in the film, such as cobalt in the form of CoPi versus cobalt as a metal. Energy dispersive X-ray spectroscopy (EDX) was used to complement the elemental analysis of the AES. Although AES is less sensitive toward the detection of heavier elements, such as selenium, EDX has higher sensitivity to these elements and can be used to confirm its presence in the hybrid material. EDX maps were taken on Ar^+ ion sputtered samples that consisted of an area including

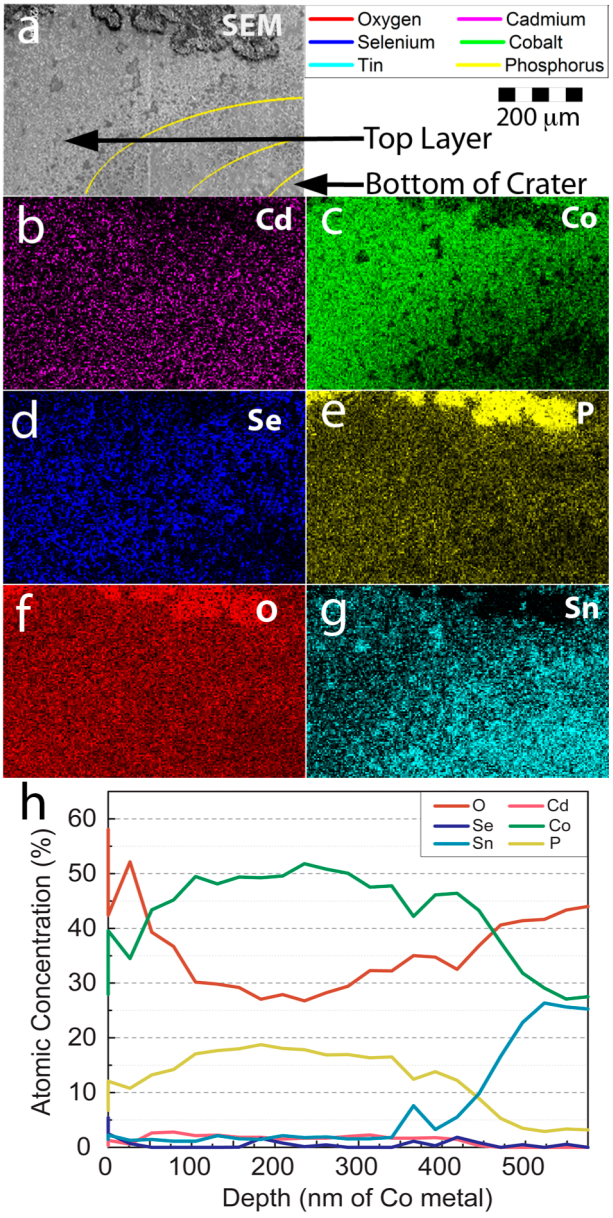

Figure 1. (a) SEM image of a crater formed by Ar^+ ion sputtering on a CdSe/CoPi electrode, with the center of the crater on the bottom right side of the image (contour lines in yellow). EDX elemental map showing the distribution of (b) cadmium, (c) cobalt, (d) selenium, (e) phosphorus, (f) oxygen, and (g) tin, respectively, throughout the entire sample. The phosphorus-rich artifact on the top of the image is a phosphate crystal formed by solution drying in the surface of the electrode, and was used as a marker for alignment of all instruments and for repeating measurements. (h) An AES elemental profile was taken while creating the crater, showing the penetration of cobalt and oxygen down to the FTO substrate layer and the presence of selenium throughout the sample.

the center of the crater, the slope, and the top layer of the sample.

An AES profile (Figure 1h) and the EDX maps (Figures 1b−g) of the crater show the elemental contents of the sample. From the elemental analysis, we detect the constituent elements of CoPi (cobalt, oxygen and phosphorus) mixed with cadmium and selenium, indicating interpenetration of photoactive CdSe and catalytic CoPi domains. This is a result of the processing of the cobalt metal to CoPi by the application

dx.doi.org/10.1021/am400364u | ACS Appl. Mater. Interfaces 2013, 5, 2364−2367

of the 1.3 V (vs Ag/AgCl) bias to the electrode. Inductively Coupled Plasma (ICP) measurements show the presence of cadmium ions in the aqueous solution following the transformation reaction, thus indicating leaching of cadmium from the innermost layer toward the surface does occur during processing. This mixing of the CoPi and CdSe materials results in a compound photoelectrode/catalyst structure. Currently, it must be noted, the elemental characterizations are unable to determine in an unequivocal manner the molecular structure of the electrode.

Catalytic and photocatalytic activities of the electrodes were electrochemically characterized using a three-electrode setup for several methods: (1) cyclic voltammetry (CV) scans in dark and illuminated conditions, (2) CV scans for extended periods of time to assess electrode stability, (3) extended-duration step potential cycles to characterize the stability of the steady state current at each potential, and (4) oxygen generation measurements under constant applied potential in dark and illuminated conditions.

Figures 2a consists of two CVs, one taken for the electrode in dark and the other with the electrode under illumination of 2 suns (Figure S4 in the Supporting Information shows the same behavior under 1 sun). The CVs in Figure 2a display a shift in the catalytic onset under illumination of the electrode; the threshold potential is lowered by 100 mV in comparison to the CV recorded in the dark. Such shifts have been observed for the application of the CoPi to other semiconductors, and this modest reduction demonstrates that the photoactivity of the electrodes, and generation of photobias, is maintained upon mixing of the CdSe and CoPi domains. Figure 2b shows the steady-state current data collected from a CdSe control electrode (red) and a CdSe/CoPi electrode (black) when poised at different potentials. The CdSe electrode passes low currents (3 μA/cm^2 at 1.25 V vs Ag/AgCl upon application of initial potential then 1 μA/cm^2 for ensuing applications). In contrast, the CdSe/CoPi photoelectrode exhibits an onset current at 1.0 V (vs Ag/AgCl) and attains an enhanced steady-state current of 1 mA/cm^2 upon operation of the photoelectrode at 1.25 V (vs Ag/AgCl). This initial activity decays to 0.5 mA/cm^2 after 19 h of cycling the bias from 0 to 1.25 V in increments of 0.25 V. The inset shows the current versus time behavior of these electrodes under the same step potentials for the initial 3 h of the measurement. Beginning at 0 V (vs Ag/AgCl) at time t = 0, the potential of the electrode is increased by increments of 0.25 V every 5 min. Each of the current spikes in the data corresponds to the application of 1.25 V (vs Ag/AgCl) and subsequent drop in the potential to 0 V vs Ag/AgCl using the same step sizes. Figure S5 in the Supporting Information shows a series of 1000 CV scans (at 50 mV/s) of a CdSe/CoPi electrode. The reproducibility of the traces demonstrates that the electrode is not modified significantly over the 6 h of operation. Figure 2c presents measurement of oxygen generation using a calibrated FOXY fluorescence probe (Ocean Optics) placed at the headspace of an airtight single cell 3-electrode setup while poising the electrode at 1.1 V (vs Ag/AgCl) under dark conditions (black) and under illumination (red); light irradiation leads to increased oxygen production. The dashed lines show that more charge passes through the system during illumination and that the increased passage of charge corresponds to oxygen production. It must be noted that this method senses only the oxygen that was released into the headspace; therefore, formation of bubbles on the electrode will not be recorded until those bubbles dislodge and rise. This

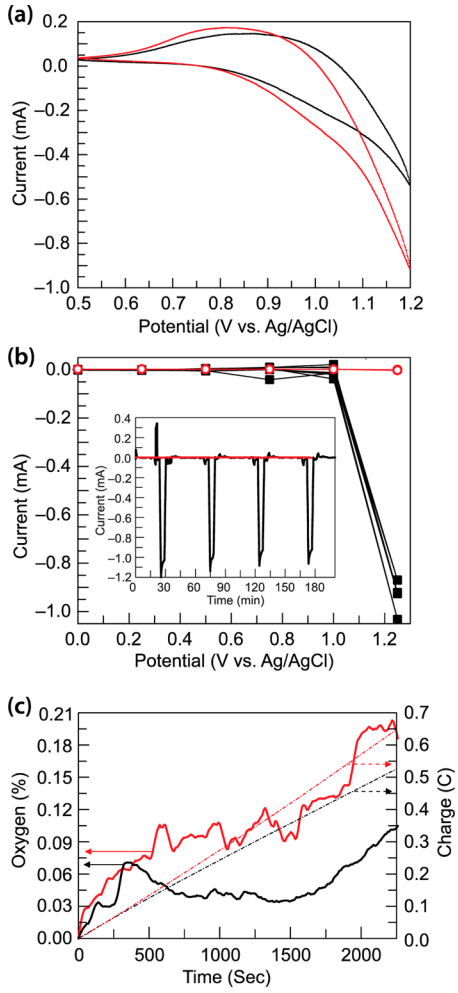

Figure 2. (a) CV at 5 mV/s showing the difference between a 1 cm^2 CdSe/CoPi electrode in the dark (black) and under 2 sun illumination (red). (b) Steady-state currents at different potentials of the CdSe/CoPi electrode (black) versus a CdSe only electrode (red), with (inset) current behavior with repetitive ramping of potential from 0 to 1.25 V and back to 0 V in increments of 0.25 V. (c) Oxygen generation of the CdSe/CoPi electrode while applying 1.1 V in dark (solid black) and under 1 sun illumination (solid red) with the respective charge passing through the system (dashed lines).

results in a noisy oxygen plot, as every dislodged bubble causes a spike in the reading. Taken together with the results of Figure 2b and Figure S2 in the Supporting Information, the CdSe/CoPi layer is stable under OER, and this stability appears to be derived from cobalt layer passivation while the electranodization of the film to form CoPi is taking place.

We demonstrate that application of a thin film of cobalt metal atop an unstable semiconductor photoanode is beneficial to the design of a photoanode for the light-assisted water splitting in two manners. First, the cobalt layer can be transformed into a catalytically active CoPi layer, by oxidation of the metal in the presence of a phosphate buffer, thus furnishing a OER catalyst. Second, the cobalt layer stabilizes the photoanode material and retards oxidation of the soft cadmium chalcogenide semiconductor under otherwise the corrosive conditions of OER. This work provides further evidence for an emerging trend[13,14] that sputtered Co thin films turned to catalysts afford protective barriers of semiconducting surfaces.

dx.doi.org/10.1021/am400364u | ACS Appl. Mater. Interfaces 2013, 5, 2364−2367

■ ASSOCIATED CONTENT

Supporting Information

Auger elemental analysis cross section of the unprocessed CdSe/Co electrode (S1), SEM images of the rough surface of the CdSe/CoPi electrodes (S2 and S3), cyclic voltammogram (CV) of CdSe/CoPi electrode under 1 sun illumination (S1) and 1000 consecutive CV scans of CdSe/CoPi electrode (S5). This material is available free of charge via the Internet at http://pubs.acs.org/.

■ AUTHOR INFORMATION

Corresponding Author

*E-mail: costi@mit.edu (R.C.); nocera@fas.harvard.edu (D.G.N.).

Present Addresses

[§]E.R.Y. is currently at Department of Chemistry, Amherst College, P.O. Box 5000, Amherst, MA 01002-5000, USA

[⊥] D.G.N. is currently at Department of Chemistry and Chemical Biology, Harvard University, 12 Oxford St., Cambridge, Massachusetts 02138-2902, USA.

Notes

The authors declare no competing financial interest.

■ ACKNOWLEDGMENTS

E.R.Y. gratefully acknowledges the National Science Foundation for an American Competitiveness in Chemistry (ACC-F) postdoctoral fellowship (Grant CHE-0936816). We thank Sun Catalytix for providing support to the ACC-F Award. We also acknowledge MIT NSF-sponsored Center for Materials Science and Engineering and MIT Microelectronics Technology Laboratory for providing us the material characterization and thin film growth tools. D.G.N. acknowledges AFOSR FA9550-09-1-0689 for support of this research.

■ REFERENCES

(1) Nozik, A. J. *Annu. Rev. Phys. Chem.* **1978**, *29*, 189−222.
(2) Heller, A. *Science* **1984**, *223*, 1141−1148.
(3) Lewis, N. S.; Nocera, D. G. *Proc. Natl. Acad. Sci. U.S.A.* **2006**, *103*, 15729−15735.
(4) Cook, T. R.; Dogutan, D. K.; Reece, S. Y.; Surendranath, Y.; Teets, T. S.; Nocera, D. G. *Chem. Rev.* **2010**, *110*, 6474−6502.
(5) Xi, L. F.; Lek, J. Y.; Liang, Y. N.; Boothroyd, C.; Zhou, W. W.; Yan, Q. Y.; Hu, X.; Chiang, F. B. Y.; Lam, Y. M. *Nanotechnology* **2011**, *22*, 275706.
(6) Cukier, R. I.; Nocera, D. G. *Annu. Rev. Phys. Chem.* **1998**, *49*, 337−369.
(7) Huynh, M. H. V.; Meyer, T. J. *Chem. Rev.* **2007**, *107*, 5004−5064.
(8) Betley, T. A.; Wu, Q.; Van Voorhis, T.; Nocera, D. G. *Inorg. Chem.* **2008**, *47*, 1849−1861.
(9) Hammes-Schiffer, S. *Acc. Chem. Res.* **2009**, *42*, 1881−1889.
(10) Kanan, M. W.; Nocera, D. G. *Science* **2008**, *321*, 1072−1075.
(11) Esswein, A. S.; Surendranath, Y.; Reece, S. Y.; Nocera, D. G. *Energy Environ. Sci.* **2011**, *4*, 499−504.
(12) Kanan, M. W.; Surendranath, Y.; Nocera, D. G. *Chem. Soc. Rev.* **2009**, *38*, 109−114.
(13) Young, E. R.; Nocera, D. G.; Bulovic, V. *Energy Environ. Sci.* **2010**, *3*, 1726−1728.
(14) Young, E. R.; Costi, R.; Paydavosi, S.; Nocera, D. G.; Bulovic, V. *Energy Environ. Sci.* **2011**, *4*, 2058−2061.
(15) Steinmiller, E. M. P.; Choi, K. S. *Proc. Natl. Acad. Sci. U.S.A.* **2009**, *106*, 20633−20636.
(16) Seabold, J. A.; Choi, K.-S. *Chem. Mater.* **2011**, *23*, 1105−1112.
(17) Zhong, D. K.; Sun, J.; Inumaru, H.; Gamelin, D. R. *J. Am. Chem. Soc.* **2009**, *131*, 6086−6087.
(18) Sun, J. W.; Zhong, D. K.; Gamelin, D. R. *Energy Environ. Sci.* **2010**, *3*, 1252−1261.
(19) Zhong, D. K.; Gamelin, D. R. *J. Am. Chem. Soc.* **2010**, *132*, 4202−4207.
(20) McDonald, K. J.; Choi, K.-S. *Chem. Mater.* **2011**, *23*, 1686−1693.
(21) Zhong, D. K.; Cornuz, M.; Sivula, K.; Graetzel, M.; Gamelin, D. R. *Energy Environ. Sci.* **2011**, *4*, 1759−1764.
(22) Pijpers, J. J. H.; Winkler, M. T.; Surendranath, Y.; Buonassisi, T.; Nocera, D. G. *Proc. Natl. Acad. Sci. U. S. A.* **2011**, *108*, 10056−10061.
(23) Reece, S. Y.; Hamel, J. A.; Sung, K.; Jarvi, T. D.; Esswein, A. J.; Pijpers, J. J. H.; Nocera, D. G. *Science* **2011**, *334*, 645−648.
(24) Coates, N. E.; Zhou, H.; Kraemer, S.; Li, L.; Moses, D. *Adv. Mater.* **2010**, *22*, 5366−5369.